# 16

# Valence Band Offsets of $ZnO/SrTiO_3$, $ZnO/BaTiO_3$, $InN/SrTiO_3$, and $InN/BaTiO_3$ Heterojunctions Measured by X-Ray Photoelectron Spectroscopy

Caihong Jia[1,2], Yonghai Chen[1], Xianglin Liu[1], Shaoyan Yang[1] and Zhanguo Wang[1]

[1]*Key Laboratory of Semiconductor Material Science, Institute of Semiconductors, Chinese Academy of Science, Beijing*

[2]*Key Laboratory of PhotovoltaicMaterials of Henan Province and School of Physics Electronics, Henan University, Kaifeng*

*China*

## 1. Introduction

The heterostructures of wurtzite semiconductors and perovskite ferroelectric oxide integrate the rich properties of perovskites together with the superior optical and electronic properties of wurtzites, thus providing a powerful method of new multifunctional devices. The electrical and optical properties of the heterostructures are strongly influenced by the interface band offset, which dictates the degree of charge carrier separation and localization. It is very important to determine the valence band offset (VBO) of semiconductor/ferroelectric oxides in order to understand the electrical and optical properties of the heterostructures and to design novel devices. In this chapter, by using X-ray photoelectron spectroscopy (XPS), we determine the VBO as well as the conduction band offset (CBO) values of the typical semiconductor/ferroelectric oxide heterojunctions, such as $ZnO/SrTiO_3$, $ZnO/BaTiO_3$, $InN/SrTiO_3$ and $InN/BaTiO_3$, that are grown by metal-organic chemical vapor deposition. Based on the values of VBO and CBO, it has been found that type-II band alignments form at the $ZnO/SrTiO_3$ and $ZnO/BaTiO_3$ interfaces, while type-I band alignments form at $InN/SrTiO_3$ and $InN/BaTiO_3$ interfaces.

For many years, heterojunctions have been one of the fundamental research areas of solid state science. The interest in this topic is stimulated by the wide applications of heterojunction in microelectronics. Devices such as heterojunction bipolar transistors, quantum well lasers and heterojunction field effect transistors (FET), already have a significant technological impact. The semiconductor-ferroelectric heterostructures have attracted much attention due to their large potential for electronic and optoelectronic device applications (Lorentz et al., 2007; Losego et al., 2009; Mbenkum et al., 2005; Voora et al., 2009; 2010). The ferroelectric constituent possesses switchable dielectric polarization, which can be exploited for modificating the electronic and optical properties of a semiconductor heterostructure. Hysteresis properties of the ferroelectric polarization allows for bistable interface polarization configuration and potentially for bistable heterostructure operation modes. Therefore, the

heterostructures of wurtzite semiconductors and perovskite ferroelectric oxides integrate the rich properties of perovskites together with the superior optical and electronic properties of wurtzites, providing a powerful method of new multifunctional devices (Peruzzi et al., 2004; Wei et al., 2007; Wu et al., 2008). It is well known that the electrical and optical properties of the heterostructures are strongly influenced by the interface band offset, which determines the barrier for hole or electron transport across the interface, and acts as a boundary condition in calculating the band bending and interface electrostatics. Therefore, it is very important to determine the valence band offset (VBO) of semiconductor/ferroelectric oxides in order to understand the electrical and optical properties of the heterostructures and to design novel devices.

Zinc oxide (ZnO) is a direct wide bandgap semiconductor with large exciton binding energy (60 meV) at room temperature, which makes it promising in the field of low threshold current, short-wavelength light-emitting diodes (LED) and laser diodes (Ozgur et al., 2005). It also has a growing application in microelectronics such as thin film transistors (TFT) and transparent conductive electrodes because of high transparency and large mobility. Indium nitride (InN), with a narrow direct band gap and a high mobility, is attractive for the near infrared light emission and high-speed/high-frequency electronic devices (Losurdo et al., 2007; Takahashi et al., 2004). Generally, ZnO and InN films are grown on foreign substrates such as *c*-plane and *r*-plane sapphire, SiC (Losurdo et al., 2007; Song et al., 2008), (111) Si and GaAs (Kryliouk et al., 2007; Murakami et al., 2008). $SrTiO_3$ (STO) single crystal is widely used as a substrate for growing ferroelectric, magnetic and superconductor thin films. Meanwhile, STO is one of the important oxide materials from both fundamental physics viewpoint and potential device applications (Yasuda et al., 2008). The electron density and hence conductivity of STO can be controlled by chemical substitution or annealing in a reducing atmosphere. Furthermore, a high-density, two-dimensional electron (hole) gas will lead to tailorable current-voltage characteristics at interfaces between ZnO or InN and STO (Singh et al., 2003). In addition, the lattice polarity of ZnO and InN (anion-polarity or cation-polarity) is expected to be controlled by the substrate polarity considering the atomic configuration of STO surface, which is also important to obtain a high-quality ZnO or InN epitaxial layer (Murakami et al., 2008). Thus, it is interesting to grow high quality wurtzite ZnO and InN films on perovskite STO substrates, and it is useful to determine the valence band offset (VBO) of these heterojunctions.

The heterojunction of semiconductor-ZnO or InN/ferroelectric-$BaTiO_3$ (BTO) provides an interesting optoelectronic application due to the anticipated strong polarization coupling between the fixed semiconductor dipole and the switchable ferroelectric dipole (Lorentz et al., 2007; Losego et al., 2009; Mbenkum et al., 2005; Voora et al., 2009; 2010). ZnO TFT, highly attractive for display applications due to transparency in the visible and low growth temperatures, are limited by large threshold and operating voltages (Kim et al., 2005). BTO, as a remarkable ferroelectric material with a high relative permittivity, can be used as the gate dielectric to reduce the operating voltages of TFT for portable applications (Kang et al., 2007; Siddiqui et al., 2006), and as an attractive candidate as an epitaxial gate oxide for field effect transistor. In addition, the free carrier concentration in the ZnO channel can be controlled by the ferroelectric polarization of BTO dielectric in the ZnO/BTO heterostructure field-effect-transistors, thus demonstrating nonvolatile memory elements (Brandt et al., 2009). In order to fully exploit the advantages of semiconductor-ferroelectric heterostructures, other combinations such as InN/BTO should be explored. As a remarkable ferroelectric material with a high relative permittivity, BTO can be used as a gate dielectric for InN based field

effect transistor. More importantly, InN/BTO heterojunction is promising for fabricating optical and electrical devices since oxidation treatment is found to reduce the surface electron accumulation of InN film (Cimalla et al., 2007). Therefore, it is important to determine the VBO of these semiconductor/ferroelectric heterojunctions to design and analyze the performance of devices.

In this chapter, we will first present several methods to determine the energy discontinuities. Then, by using x-ray photoelectron spectroscopy (XPS), we determine the VBO as well as the conduction band offset (CBO) values of the typical semiconductor/ferroelectric oxide heterojunctions, such as ZnO/STO, ZnO/BTO, InN/STO, and InN/BTO, that are grown by metal-organic chemical vapor deposition. Based on the values of VBO and CBO, it has been found that type-II band alignments form at the ZnO/STO and ZnO/BTO interfaces, while type-I band alignments form at the InN/STO and InN/BTO interfaces.

## 2. Measurement methods

The energy band edge discontinuities at heterostructures can be determined by applying a large variety of experimental techniques, such as electrical transport measurements including capacitance-voltage (C-V) and current-voltage (I-V), optical measurement, photoemission measurement (Capasso et al., 1987). For many years, analysis of the capacitance-voltage and current-voltage of heterojunctions have proven to be important probes for determining the energy barriers of pn junction, Schottky barriers and heterojunctions. The energy discontinuities can be determined by C-V measurement, since the C(V) function has the form of:

$$C = \frac{2(\epsilon_1 N_1 + \epsilon_2 N_2)}{q\epsilon_1\epsilon_2 N_1 N_2}(V_D - V)^{-1/2}, \tag{1}$$

where $\epsilon_1$ and $\epsilon_2$ are the dielectric constants of materials 1 and 2, $N_1$ and $N_2$ are the dopant concentrations of materials 1 and 2, $V_D$ is the diffusion potential, while q is the electronic charge. Therefore, the plot of $C^{-2}$ versus V gives a straight line, intercepting the V-axis exactly at $V=V_D$. Based on this quantity, the conduction band discontinuity energy, $\Delta E_c$, can be obtained to be

$$\Delta E_c = qV_D + \delta_2 - (E_{g1} - \delta_1), \tag{2}$$

for anisotype pN heterojunctions; and

$$\Delta E_c = qV_D + \delta_2 - \delta_1, \tag{3}$$

for isotype nN heterojunctions. Where $\delta_1$ and $\delta_2$ refer to the position of the Fermi energies relative to the conduction band minimum (or valence band maximum) in n (or p)-type materials 1 and 2, respectively. That is,

$$\delta_i = kTln(\frac{N_{ci}}{N_i}), i = 1, 2. \tag{4}$$

Here, kT is the Boltzmann energy at the temperature T, $N_{ci}$ is the effective conduction band density of states,

$$N_c = \frac{2(2\pi m^* kT)^{\frac{3}{2}}}{h^3}, \tag{5}$$

which is a function of the reduced effective mass of the electron ($m^*$) and of temperature (T). Therefore, the difference in the Fermi energies between materials 1 and 2 can be simplified to give

$$\delta_2 - \delta_1 = kTln(\frac{N_{D1}}{N_{D2}}) + \frac{3}{2}kTln(\frac{m_2^*}{m_1^*}), \quad (6)$$

for an nN heterojunction. Thus once the diffusion potential $V_D$ is determined, it is relatively straightforward to obtain the conduction band discontinuity. Indeed, as can be seen from the equation above, it is not necessary to have a highly precise measurement of any of the material parameters such as the bulk free carrier concentration or the effective density of states, since $\Delta E_c$ depends only logarithmically on these parameters. On the other hand, the dependence of $\Delta E_c$ on $V_D$ is linear, and, therefore, it is important that the measurement of the diffusion potential be as accurate as possible.
The current density is given simply by

$$J = A^* T^2 exp(-\frac{q\phi_B}{kT}), \quad (7)$$

where $\phi_B$ is the barrier height, from which the energy band offset can be determined. The transport measurements have the advantage of being a relatively understanding means of acquiring data using simple structures, but the accuracy of these techniques has never been considered to be particularly high, basically due to the existence of parasitic phenomena giving rise to excess stray capacitances or dark currents, which introduces variables cannot be easily treated in the overall analysis and confuse the measurements.
The optical measurement techniques are based on the study of the optical properties of alternating thin layers of two semiconductors. The quantized energy levels associated with each well depend on the corresponding discontinuity, on the width of the well and on the effective mass. The processes involving the localized quantum well states will introduce series of peaks both in the absorption and photoluminescence spectra. From the position in energy of the peaks in each series, it is possible to retrieve the parameters of the well and in particular the value of $\Delta E_C$ and $\Delta E_V$. However, this approach requires the fabrication of high-quality multilayer structures with molecular beam epitaxy, and can only be applied to nearly ideal interface with excellent crystal quality.
For x-ray photoelectron spectroscopy (XPS), it is well established that the kinetic energy, $E_K$, of electrons emitted from a semiconductor depends on the position of the Fermi level, $E_F$, within the semiconductor band gap. This aspect of XPS makes it possible to determine $E_F$ relative to the valence band maximum, $E_V$, in the region of the semiconductor from which the photoelectron originate. Therefore, besides analyzing the interface elemental and chemical composition, XPS can also be used as a contactless nondestructive and direct access to measure interface potential related quantities such as heterojunction band discontinuites. This technique was pioneered by Grant ea al (Grant et al., 1978). Since the escape depths of the respective photoelectrons are in the order of 2 nm only, one of the two semiconductors has to be sufficiently thin. This condition may be easily met when heterostructures are grown by molecular beam epitaxy (MBE) or metal-organic chemical vapor deposition (MOCVD). The XPS method for determining VBO is explained by the schematic band diagram displayed in Fig. 1, in which an idealized flat band was assumed. Based on the measured values of $\Delta E_{CL}$, the core level to $E_V$ binding energy difference in bulk semiconductors A and B, ($E_{CL}^A$-$E_V^A$) and

($E^B_{CL}$-$E^B_V$), respectively. By inspection of Fig. 1, it can be seen that

$$\Delta E_V(B - A) = (E^B_{CL} - E^B_V) - (E^A_{CL} - E^A_V) + \Delta E_{CL}(A - B). \quad (8)$$

Thus, to apply XPS for $\Delta E_V$ measurements, it is essential to determine the bulk semiconductor material parameters ($E_{CL}$-$E_V$) for those semiconductors forming the heterojunctions. A primary difficulty with measuring ($E_{CL}$-$E_V$) is the accurate determination of the $E_V$ position in photoemission spectra. The most frequently employed method involves extrapolation of a tangent line to the leading edge of the valence band spectrum to the energy axis, this intercept is defined as $E_V$. Substituting these values to Eq. 8, the VBO of heterojunction A/B can be obtained.

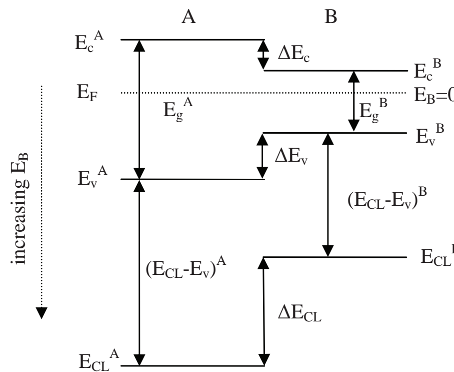


Fig. 1. Schematic energy band diagram illustrating the measurement of VBO by XPS.

## 3. Experimental

Several samples, bulk commercial (001) STO, (111) STO and (001) BTO substrates, thick (several hundred nanometers) and thin (about 5 nm) ZnO and InN layers grown on the commercial STO and BTO substrates were studied in this work. To get a clean interface, the STO and BTO substrates were cleaned with organic solvents and rinsed with de-ionized water sequentially before loading into the reactor. The thick and thin heterostructures of ZnO/STO, ZnO/BTO, InN/STO and InN/BTO were deposited by MOCVD. More growth condition details of the ZnO and InN layers can be found in our previous reports (Jia et al., 2008; 2009a;b; 2010a;b; 2011; Li et al., 2011).

XPSs were performed on ThermoFisher ESCALAB 250, PHI Quantera SXM, and VG MKII XPS instruments with AlK$\alpha$ (h$\nu$=1486.6 eV) as the x-ray radiation source, which had been carefully calibrated on work function and Fermi energy level ($E_F$). Because all the samples were exposed to air, there must be some impurities (e.g., oxygen and carbon) existing in the sample surface, which may prevent the precise determination of the positions of the valence band maximum (VBM). To reduce the undesirable effects of surface contamination, all the samples were cleaned by $Ar^+$ bombardment at a low sputtering rate to avoid damage to the samples. After the bombardment, peaks related to impurities were greatly reduced, and no new peaks appeared. Because a large amount of electrons are excited and emitted from the sample, the sample is always positively charged and the electric field caused by the charge can affect the measured kinetic energy of photoelectron. Charge neutralization was performed

with an electron flood gun and all XPS spectra were calibrated by the C 1s peak at 284.8 eV from contamination to compensate the charge effect. Since only the relative energy position in each sample is needed to determine the VBO, the absolute energy calibration for a sample has no effect on the ultimate result. The surfaces of samples were examined initially by low-resolution survey scans to determine which elements were present. Very high-resolution spectra were acquired to determine the binding energy of core level (CL) and the valence band maximum energy in the survey spectra. All the CL spectra were fitted to Voigt (mixed Lorentz-Gaussian) line shape with a Shirley background. Since considerable accordance of the fitted line to the original measured data has been obtained, the uncertainty of the CL position should be less than 0.03 eV, as evaluated by numerous fittings with different parameters. The VBM positions in the valence band (VB) spectra were determined by linear extrapolation of the leading edge of the VB spectra recorded on bulk substrates and thick films to the base lines in order to account for instrument resolution induced tail (Zhang et al., 2007), which has already been widely used to determine the VBM of semiconductors. Evidently, the VBM value is sensitive to the choice of points on the leading edge used to obtain the regression line (Chambers et al., 2001). Thus, several different sets of points were selected over the linear region of the leading edge to perform regressions, and the uncertainty of VBO is found to be less than 0.06 eV in the present work.

## 4. VBO for ZnO/STO heterojunction

Figure 2 (a) shows the x-ray $\theta$-2$\theta$ diffraction patterns of thick ZnO films on (111) STO substrates. The diffractogram indicates only a single phase ZnO with a hexagonal wurtzite structure. Only peaks of ZnO (0002) and (0004) reflection and no other ZnO related peaks are observed, implying a complete *c*-axis oriented growth of the ZnO layer. The highly oriented ZnO films on STO substrate strongly suggest that the nucleation and crystal growth is initiated near the substrate surface. The full width at half maximum (FWHM) of symmetric (0002) scan is about 0.85° along $\omega$-axis, as shown in the inset of Fig. 2(a). X-ray off-axis $\phi$ scans are performed to identify the in-plane orientation relationships between the film and substrate. The number of peaks in a $\phi$ scan corresponds to the number of planes for a particular family that possesses the same angle with the film surface. Figure 2 (b) shows the results of x-ray $\phi$ scans performed using the $\{11\bar{2}2\}$ reflection of ZnO (2$\theta$=67.95°, $\chi$=58.03°) and the {110} reflection of STO (2$\theta$=32.4°, $\chi$=35.26°). Only six peaks separated by 60° are observed for the ZnO {112} family, which has six crystal planes with the same angle with the growth plane ($\chi$=58.03°), as shown in Fig. 2 (b), indicating a single domain. From the relative position of ZnO {112} and STO {110} families, the in-plane relationships can be determined to be $[11\bar{2}0]$ZnO$\|$$[0\bar{1}1]$STO. The atomic arrangement in the (0001) basal plane of ZnO is shown in Fig. 2 (c). The growth in this direction shows a large lattice mismatch of about 17.7% ($\frac{2a_{ZnO}-\sqrt{2}a_{STO}}{\sqrt{2}a_{STO}}\times 100\%$) along the direction of $<11\bar{2}0>_{ZnO}$, although it shows a much smaller lattice mismatch of 1.91% ($\frac{\sqrt{3}a_{ZnO}-\sqrt{2}a_{STO}}{\sqrt{2}a_{STO}}\times 100\%$) along the direction of $<1\bar{1}00>_{ZnO}$ when ZnO rotated 30° in plane.

For ZnO/STO heterojunction, the VBO ($\Delta E_V$) can be calculated from the formula

$$\Delta E_V = \Delta E_{CL} + (E_{Zn2p}^{ZnO} - E_{VBM}^{ZnO}) - (E_{Ti2p}^{STO} - E_{VBM}^{STO}), \quad (9)$$

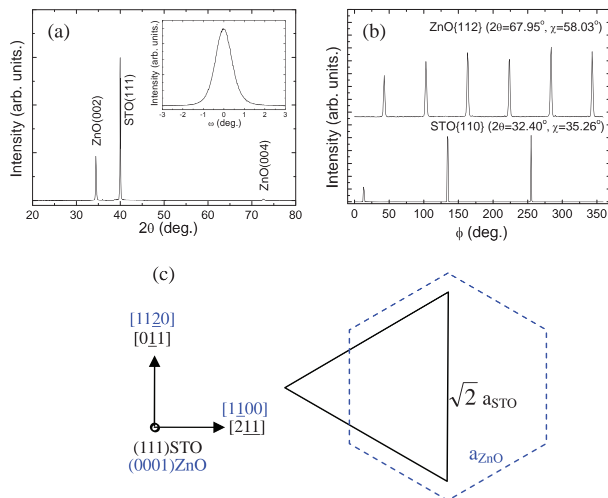


Fig. 2. X-ray $\theta$-$2\theta$ (a), $\omega$ (inset of (a)), and $\phi$ (b) scans and atomic arrangement (c) of ZnO films on (111) STO substrate.

where $\Delta E_{CL}$=($E^{ZnO/STO}_{Ti2p}$-$E^{ZnO/STO}_{Zn2p}$) is the energy difference between Zn 2p and Ti 2p CLs measured in the thin ZnO/STO heterojunction sample, and ($E^{STO}_{Ti2p}$-$E^{STO}_{VBM}$) and ($E^{ZnO}_{Zn2p}$-$E^{ZnO}_{VBM}$) are the VBM energies with reference to the CL positions of bulk STO and thick ZnO film, respectively, which are obtained by XPS measurement from the respective STO substrate and thick ZnO film.
Figure 3 shows the XPS Ti 2p and Zn 2p CL narrow scans and the valence band spectra from the STO substrate and the thick ZnO/STO samples, respectively. As shown in Fig. 3(a), the Zn 2p CL peak locates at 1021.69$\pm$0.03 eV. Fig. 3(e) shows the VB spectra of the thick ZnO sample, and the VBM position is determined to be 1.06$\pm$0.06 eV by a linear fitting depicted above. As a result, the energy difference of Zn 2p to ZnO VBM ($E^{ZnO}_{Zn2p}$-$E^{ZnO}_{VBM}$) can be determined to be 1020.63$\pm$0.03 eV. Using the same Voigt fitting and linear extrapolation methods mentioned above, the energy difference of Ti2p to STO VBM ($E^{STO}_{Ti2p}$-$E^{STO}_{VBM}$) can be determined to be 457.32$\pm$0.06 eV. The CL spectrum of Zn 2p and Ti 2p in thick ZnO film and bulk STO are quite symmetric indicating the uniform bonding state and the only peaks correspond to Zn-O and Ti-O bonds, respectively. The measurement of $\Delta E_{CL}$ for the Ti 2p and Zn 2p CLs recorded in the thin ZnO/STO junction is illustrated in Fig. 3(c) and (d). After substraction of the background, the spectra of Ti 2p and Zn 2p CLs were well Voigt fitted and the energy difference of Ti 2p and Zn 2p CLs ($\Delta E_{CL}$) can be determined to be 562.69$\pm$0.03 eV. It is noteworthy that the Ti 2p peak is not symmetric and consists of two components by careful Voigt fitting. The prominent one located at 459.22 eV is attributed to the Ti emitters within the STO substrate which have six bonds to oxygen atoms, and the other one shifting by $\sim$2 eV to a lower binding energy indicates the presence of an interfacial oxide layer. This phenomenon is similar to that observed in the interface of $LaAlO_3/SrTiO_3$, and the shoulder at lower binding energy is attributed to $TiO_x$ suboxides, which is expected on account of the $TiO_x$-terminated STO initial surface (Kazzi et al., 2006). The fair double-peak fitting shown

in Fig. 3(d) confirms the presence of $TiO_x$ suboxides. Substituting the above ($E^{STO}_{Ti2p}$-$E^{STO}_{VBM}$), ($E^{ZnO}_{Zn2p}$-$E^{ZnO}_{VBM}$) and $\Delta E_{CL}$ into Eq. 9, the resulting VBO value is calculated to be 0.62±0.09 eV.

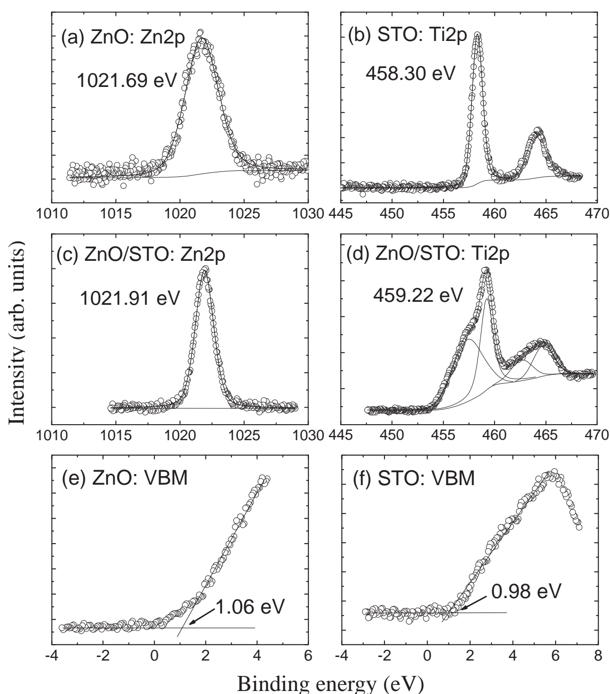


Fig. 3. Zn 2p spectra recorded on ZnO (a) and ZnO/STO (c), Ti 2p spectra on STO (b) and ZnO/STO (d), and VB spectra for ZnO (e) and STO (f). All peaks have been fitted to Voigt line shapes using Shirley background, and the VBM values are determined by linear extrapolation of the leading edge to the base line. The errors in the peak positions and VBM are ±0.03 and ±0.06 eV, respectively.

The reliability of the measured result is analyzed by considering several possible factors that could impact the experiment results. The lattice mismatch between ZnO and STO is about ∼17.7%, which will induce a much smaller critical thickness than 5-10 nm, compared with the lattice mismatch of $BaTiO_3$ grown on STO (2.2%) and a critical thickness of 5-10 nm (Sun et al., 2004). Meanwhile, the ZnO epitaxial layer grown on STO substrate by MOCVD is characterized by columnar growth mode, which provides strain relief mechanism (Fan et al., 2008). Thus, the ZnO overlayer in the heterojunction is almost completely strained and the strain-induced piezoelectric field effect can also be neglected. In addition, the error induced by band bending is checked to be much smaller than the average standard deviation of ±0.09 eV given above (Yang et al., 2009). Since the factors that can affect the ultimate result can be excluded from the measured result, the experimental obtained VBO value is reliable.
To further confirm our result, it would be very useful to compare our experimental results with a theoretical model proposed by Mönch (Monch et al., 2005). The VBOs of ZnO heterojunctions are predicted based on the difference of the respective interface-induced gap

states (IFIGS) branch-point energies and electric dipole terms. That is

$$\Delta E_V = E_{vl}(\Gamma) - E_{vr}(\Gamma) = \phi^p_{bpr} - \phi^p_{bpl} + D_X(X_{sr} - X_{sl}), \tag{10}$$

where the p-type branch-point energy $\phi^p_{bp}(\Gamma) = E_{bp} - E_V(\Gamma)$ is the energy distance from the valence band maximum to the branch point of the IFIGS and $X_s$ is the electronegativity of the respective semiconductor. The subscripts $r$ and $l$ stand for the right and left side, respectively, of the heterostructure. The dipole parameter $D_X$ is determined by the density of states and extension of the IFIGS at their branch point. This dipole term can also be neglected, just like the common semiconductor heterojunctions, since the electronegativities of the atoms constituting ZnO/STO heterojunction differ by up to 10% only. Through analysis of the VBO values reported for ZnO heterostructure (Monch et al., 2005), the dependence of VBO on the p-type branch-point energy is obtained to be

$$\Delta E_V = \varphi_{vbo}[\phi^p_{bp}(ZnO) - \phi^p_{bp}(semi)]. \tag{11}$$

With the p-type branch-point energies of ZnO (3.04 eV) (Monch et al., 2005) and STO (2.5 eV) (Monch et al., 2004), and the slope parameters $\varphi_{vbo}$ for insulator heterostructures of 1.14$\sim$1.23, a VBO of 0.64$\pm$0.21 eV would be calculated, which is in good agreement with the experimentally determined value of 0.62$\pm$0.09 eV. It implies that the IFIGS theory is not only widely used to the group-IV elemental semiconductors, SiC, and the III-V, II-VI, and I-III-$VI_2$ compound semiconductors and their alloys (Monch et al., 2005), but also applicable to the semiconductor/insulator heterostructures. In addition, the resulting $\Delta E_V$ is a sufficiently large value for device applications in which strong carrier confinement is needed, such as light emitters or heterostructure field effect transistors. For instance, the valence band offset in the $Zn_{0.95}Cd_{0.05}O$/ZnO system is only 0.17 eV (Chen et al., 2005), which is less than that of ZnO/STO.

Finally, the CBO ($\Delta E_C$) can be estimated by the formula $\Delta E_C = \Delta E_V + E_g^{ZnO} - E_g^{STO}$. By substituting the band gap values ($E_g^{ZnO}$=3.37 eV (Su et al., 2008) and $E_g^{STO}$=3.2 eV (Baer et al., 1967)), $\Delta E_C$ is calculated to be 0.79$\pm$0.09 eV. It would be interesting to compare our experimental values with the electrical transport results by Wu et al (Wu et al., 2008). They have investigated the temperature dependent current-voltage characteristic of ZnO/Nb:$SrTiO_3$ junction, and found that the effective barrier height ($\phi_{eff}$) is 0.73 eV, which is directly considered to be the CBO in n-N heterojunctions (Alivov et al., 2006). It can be seen that the effective barrier height in Wu's work is consistent with our CBO value. Accordingly, a type-II band alignment forms at the heterojunction interface, in which the conduction and valence bands of the ZnO film are concomitantly higher than those of the STO substrate, as shown in Fig. 4.

## 5. VBO for ZnO/BTO heterojunction

In x-ray $\theta$-$2\theta$ diffraction measurements, as shown in Fig. 5 (a), the ZnO/BTO sample presented the only peak of ZnO (0002) reflection and no other ZnO related peaks were observed, implying a complete *c*-axis oriented growth of the ZnO layer. From the pole figure of ZnO $\{10\bar{1}1\}$ family, shown in Fig. 5 (b), twelve peaks separated by 30° are present, although ZnO has a sixfold symmetry about the [0001] axis, indicating that the ZnO film is twinned in the growth plane by a 30° in-plane rotation. The relative intensities of the two sets of peaks is

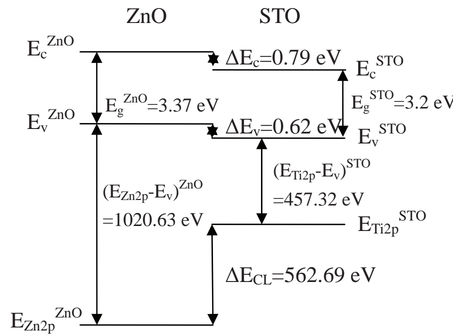


Fig. 4. Energy band diagram of ZnO/STO heterojunction.

related to the proportion of the two domains, indicating that the two domains are almost equal in amount.

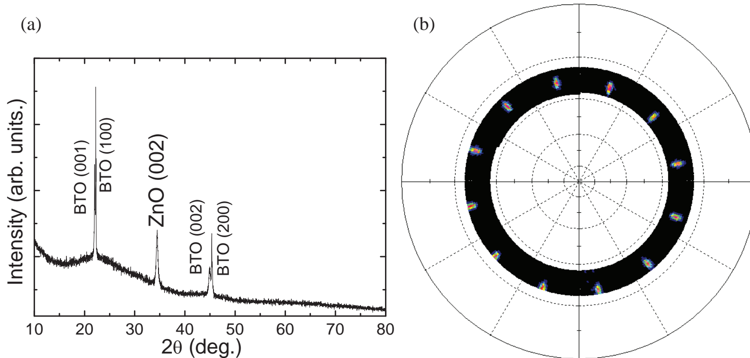


Fig. 5. X-ray $\theta$-$2\theta$ diffraction pattern (a) and pole figure (b) of the thick ZnO films on BTO substrates.

For ZnO/BTO heterojunction, the VBO ($\Delta E_V$) can be calculated from the formula

$$\Delta E_V = \Delta E_{CL} + (E_{Zn2p}^{ZnO} - E_{VBM}^{ZnO}) - (E_{Ti2p}^{BTO} - E_{VBM}^{BTO}), \tag{12}$$

where $\Delta E_{CL}$=($E_{Ti2p}^{ZnO/BTO}$-$E_{Zn2p}^{ZnO/BTO}$) is the energy difference between Zn 2p and Ti 2p CLs measured in the thin ZnO/BTO heterojunction, while ($E_{Ti2p}^{BTO}$-$E_{VBM}^{BTO}$) and ($E_{Zn2p}^{ZnO}$-$E_{VBM}^{ZnO}$) are the VBM energies with reference to the CL positions of bulk BTO and thick ZnO film, respectively. Figure 6 shows the XPS Ti 2p and Zn 2p CL narrow scans and the valence band spectra from the bulk BTO, thick and thin ZnO/BTO samples, respectively. For the thick ZnO film, the Zn 2p CL peak locates at 1022.04±0.03 eV, and the VBM position is determined to be 2.44±0.06 eV by a linear fitting described above, as shown in Fig. 6(a) and (e). The energy difference between Zn 2p and VBM of thick ZnO film ($E_{Zn2p3}^{ZnO}$-$E_{VBM}^{ZnO}$) is deduced to be 1019.60±0.09 eV, which is well consistent with our previous reports (Zhang et al., 2007). It can also be clearly seen from Fig. 6 that the CL spectra of Zn 2p and Ti 2p in the thick ZnO film and thin ZnO/BTO heterojunction are quite symmetric, indicating a uniform bonding state and

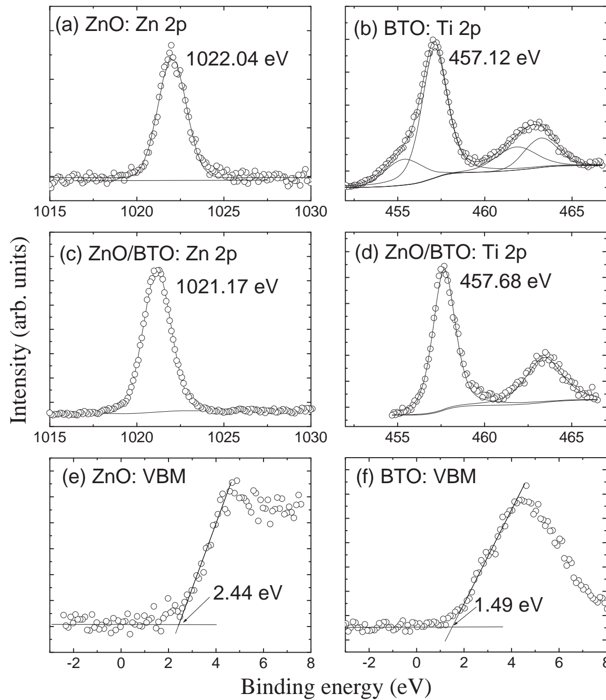


Fig. 6. Zn 2p spectra recorded on ZnO (a) and ZnO/BTO (c), Ti 2p spectra on BTO (b) and ZnO/BTO (d), and VB spectra for ZnO (e) and BTO (f). All peaks have been fitted to Voigt line shapes using Shirley background, and the VBM values are determined by linear extrapolation of the leading edge to the base line. The errors in the peak positions and VBM are ±0.03 and ±0.06 eV, respectively.

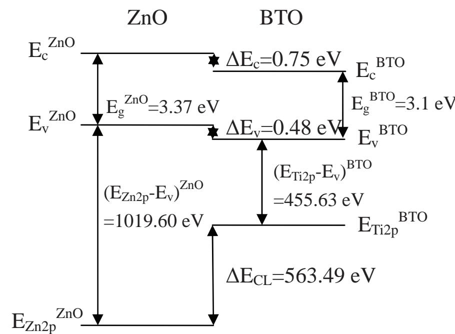


Fig. 7. Energy band diagram of ZnO/BTO heterojunction.

the only peaks correspond to Zn-O and Ti-O bonds, respectively. However, the Ti 2p peak in the bulk BTO is not symmetric and consists of two components by careful Voigt fitting. The prominent one located at 457.12±0.03 eV is attributed to the Ti emitters within the BTO substrate, which have six bonds to oxygen atoms. The other one shifting by ∼2 eV to a lower

binding energy is attributed to $TiO_x$ suboxides on account of the TiO-terminated BTO initial surface (Kazzi et al., 2006). It is interesting that the Ti 2p peaks transform from asymmetry in bulk BTO to symmetry in the thin ZnO/BTO sample, implying that the $TiO_x$ suboxides in the BTO surface is oxidized completely to the highest valence of $Ti^{4+}$. The VBM value of bulk BTO is determined to be 1.49±0.06 eV using the linear method. The Fermi level of an insulator is expected to be located in the middle of the forbidden energy gap, so the VBM will be one-half of the band gap of insulators (You et al., 2009). For BTO, the VBM should be 1.55 eV calculated from the band gap of 3.1 eV (Boggess et al., 1990), which is in good agreement with the measured value (1.49±0.06 eV) in the present work. Using the same fitting methods mentioned above, the energy values of CL for the thin ZnO/BTO heterojunction can be determined, as shown in Fig. 6. Substituting the above values into Eq. 12, the resulting VBO value is calculated to be 0.48±0.09 eV.

A small lattice mismatch is present between the BTO[$0\bar{1}1$] direction and the hexagonal apothem of ZnO, which is only about 0.8% ($\frac{\sqrt{3}a_{ZnO}-\sqrt{2}a_{BTO}}{\sqrt{2}a_{BTO}}\times 100\%$) (Wei et al., 2007). This lattice mismatch is so small that the strain-induced piezoelectric field effect can be neglected in this work (Su et al., 2008). In ZnO/MgO heterostructure, the 8.3% mismatch brings a shift of 0.22 eV on VBO (Li et al., 2008). By linear extrapolation method, the strain induced shift in ZnO/BTO is less than 0.02 eV, which is much smaller than the aforementioned deviation of 0.09 eV. The error induced by band bending is checked to be much smaller than the average standard deviation of 0.09 eV given above (Yang et al., 2009). So the experimental obtained VBO value is reliable.

To further confirm the reliability of the experimental values, it would be useful to compare our VBO value with other results deduced by transitive property. For heterojunctions formed between all pairs of three materials (A, B, and C), $\Delta E_V$(A-C) can be deduced from the difference between $\Delta E_V$(A-B) and $\Delta E_V$(C-B) neglecting the interface effects (Foulon et al., 1992). The reported VBO values for some heterojunctions are $\Delta E_V$(ZnO-STO)=0.62 eV (Jia et al., 2009b), $\Delta E_V$(Si-STO)=2.38 or 2.64 eV, and $\Delta E_V$(Si-BTO)=2.35 or 2.66 eV (Amy et al., 2004), respectively. Then the $\Delta E_V$(ZnO-BTO) is deduced to be 0.59, 0.64, 0.9 or 0.33 eV, which is comparable to our measured value 0.48±0.09 eV. Since the samples were prepared under different growth conditions, the different interfaces are responsible for the difference between our measured value and the results from the transitivity. In addition, the resulting $\Delta E_V$ is a sufficiently large value for device applications which require strong carrier confinement, such as light emitters or heterostructure field effect transistors (Chen et al., 2005).

Finally, the CBO ($\Delta E_C$) can be estimated by the formula $\Delta E_C=\Delta E_V+E_g^{ZnO}-E_g^{BTO}$. By substituting the band gap values at room temperature ($E_g^{ZnO}$=3.37 eV (Su et al., 2008) and $E_g^{BTO}$=3.1 eV (Boggess et al., 1990)), $\Delta E_C$ is calculated to be 0.75±0.09 eV. Accordingly, a type-II band alignment forms at the heterojunction interface, in which the conduction and valence bands of the ZnO film are concomitantly higher than those of the BTO substrate, as shown in Fig. 7.

## 6. VBO for InN/STO heterojunction

Figure 8 (a) shows the typical XRD $\theta$-$2\theta$ patterns of InN thin films deposited on (001) STO substrates. InN crystals shows an intense diffraction line at $2\theta$=31.28° assigned to the (0002) diffraction of InN with hexagonal wurtzite structure, implying that the *c*-axis of InN films is perpendicular to the substrate surface. Figure 8 (b) shows the results of x-ray off-axis

$\phi$ scans performed using the $\{10\bar{1}1\}$ reflection of InN ($2\theta$=33.49°, $\chi$=61.86°) and the {111} reflection of STO ($2\theta$=39.96°, $\chi$=54.74°) to determine the in-plane orientation of the InN film relative to STO. Although InN has a sixfold symmetry about the [0001] axis, the presence of twelve peaks separated by 30° for $\{11\bar{2}2\}$ reflections indicates that the InN films is twinned in the growth plane by a 30° in-plane rotation. The relative intensities of the two sets of peaks is related to the proportion of the two domains, indicating almost the same amount for the two domains. Comparing the locations in $\phi$-space of the InN$\{10\bar{1}1\}$ with STO{111} families, the two-dimensional epitaxial relationships for the two domains can be derived to be $[1\bar{1}00]$InN$\|$[110]STO for one domain and $[11\bar{2}0]$InN$\|$[110]STO for the other. The atomic arrangements for the two domains are illustrated in the schematic drawings of Fig. 8(c).

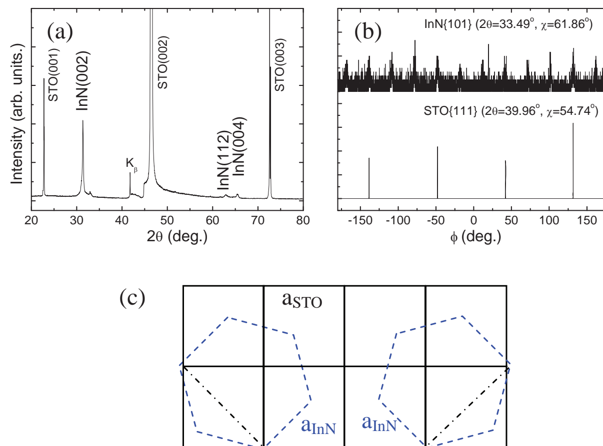


Fig. 8. X-ray $\theta$-$2\theta$ (a) and $\phi$ (b) scanning patterns, and atomic arrangement (c) of the thick InN films on (001)STO substrates.

For InN/STO heterojunction, the VBO ($\Delta E_V$) can be calculated from the formula

$$\Delta E_V = \Delta E_{CL} + (E^{InN}_{In3d} - E^{InN}_{VBM}) - (E^{STO}_{Ti2p} - E^{STO}_{VBM}), \tag{13}$$

where $\Delta E_{CL}$=($E^{InN/STO}_{Ti2p}$-$E^{InN/STO}_{In3d}$) is the energy difference between In 3d and Ti 2p CLs measured in the thin InN/STO heterojunction, while ($E^{STO}_{Ti2p}$-$E^{STO}_{VBM}$) and ($E^{InN}_{In3d}$-$E^{InN}_{VBM}$) are the VBM energies with reference to the CL positions of bulk STO and thick InN film, respectively. Fig. 9 shows In 3d, Ti 2p CL narrow scans and valence band spectra recorded on thick InN, bulk STO and thin InN/STO heterojunction samples, respectively. The In 3d spectra in thick InN films include two peaks of $3d_{5/2}$ (443.50±0.03 eV) and $3d_{3/2}$ (451.09±0.03 eV), which are separated by the spin-orbit interaction with a splitting energy of around 7.57 eV. Both peaks are found out to consist of two components by careful Voigt fitting. The first In $3d_{5/2}$ component located at 443.50±0.03 eV is attributed to the In-N bonding, and the second, at 444.52±0.03 eV, is identified to be due to surface contamination. This two-peak profile of the In $3d_{5/2}$ spectra in InN is typical and have been demonstrated by other researchers (King et al., 2008; Piper et al., 2005; Yang et al., 2009). Comparison of their binding energy separation with previous results, we suggest that the second peak at 444.52±0.03 eV to the In-O bonding is due to contamination by oxygen during the growth process. The ratio of In-N peak intensity to

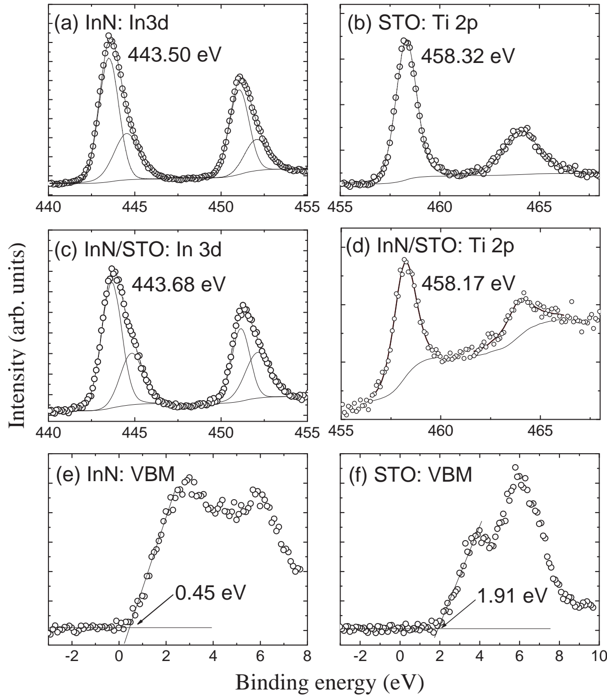


Fig. 9. In 3d spectra recorded on InN (a) and InN/STO (c), Ti 2p spectra on STO (b) and InN/STO (d), and VB spectra for InN (e) and STO (f). All peaks have been fitted to Voigt line shapes using Shirley background, and the VBM values are determined by linear extrapolation of the leading edge to the base line. The errors in the peak positions and VBM are ±0.03 and ±0.06 eV, respectively.

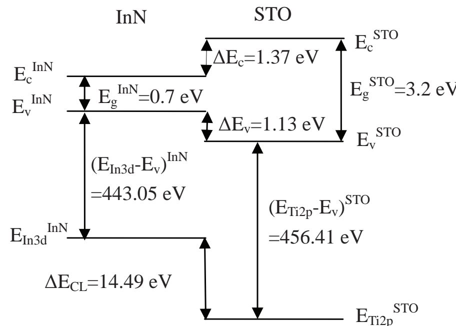


Fig. 10. Energy band diagram of InN/STO heterojunction.

the oxygen related peaks indicates that only a small quantity of oxygen contamination exists in our samples. Both the Ti 2p spectra in bulk STO and thin InN/STO heterojunction are quite symmetric, indicating a uniform bonding state. Using the linear extrapolation method mentioned above, the VBM of InN and STO are 0.45±0.06 eV and 1.91±0.06 eV respectively.

Compared with the spectra recorded on the InN and STO samples, the In 3d core level shifts to 443.68±0.03 eV and Ti 2p shifts to 458.17±0.03 eV in thin InN/STO heterojunction. The VBO value is calculated to be 1.13±0.09 eV by substituting those values into Eq. 13.
Reliability of the analysis of the measured results is provided by considering possible factors that could impact the experimental results. InN is a kind of piezoelectric crystal, so the strain existing in the InN overlayer of the heterojunction will induce piezoelectric field and affect the results. The lattice mismatch between InN and STO is larger than 9.8% ($\frac{\sqrt{3}a_{InN}-\sqrt{2}a_{STO}}{\sqrt{2}a_{STO}} \times 100\%$), so the InN layer can be approximately treated as completely relaxed and this approximation should not introduce much error in our result. In addition, the energy band bends downward at the surface of InN film and there is an electron accumulation layer (Mahboob et al., 2004), so the energy separation between VBM and Fermi level can be changed at the InN surface, which could impact the measured VBO values of the heterojunctions. However, both the CL emissions of In 3d and Ti 2p at the InN/STO heterojunction are collected from the same surface (InN surface), thus, the surface band bending effects can be canceled out for the measurement of $\Delta E_{CL}$, as was the measurement of the band offset of the InN/AlN heterojunction by others (King et al., 2007; Wu et al., 2006). Since the factors that can affect the results can be excluded from the measured results, the experimental obtained VBO value is reliable.
Making use of the band gap of InN (0.7 eV) (Yang et al., 2009) and SrTiO$_3$ (3.2 eV) (Baer et al., 1967), the CBO ($\Delta E_C$) is calculated to be 1.37 eV and the ratio of $\Delta E_C/\Delta E_V$ is close to 1:1. As shown in Fig. 10, a type-I heterojunction is seen to be formed in the straddling configuration. So STO can be utilized as the gate oxide for InN based metal-oxide semiconductor, the gate leakage is expected to be negligible, which is different from the Si based devices (Chambers et al., 2000).

## 7. VBO for InN/BTO heterojunction

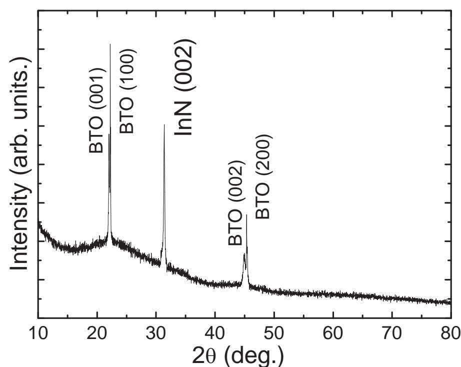


Fig. 11. X-ray $\theta$-2$\theta$ scanning patterns of the thick InN films on BTO substrates.

In x-ray $\theta$-2$\theta$ diffraction measurements, as shown in Fig. 11, the thick InN/BTO sample presented the only peak of InN (0002) reflection and no other InN related peaks were observed, implying a complete *c*-axis oriented growth of the InN layer. For InN/BTO heterojunction, the VBO ($\Delta E_V$) can be calculated from the formula

$$\Delta E_V = \Delta E_{CL} + (E^{InN}_{In3d} - E^{InN}_{VBM}) - (E^{BTO}_{Ti2p} - E^{BTO}_{VBM}), \quad (14)$$

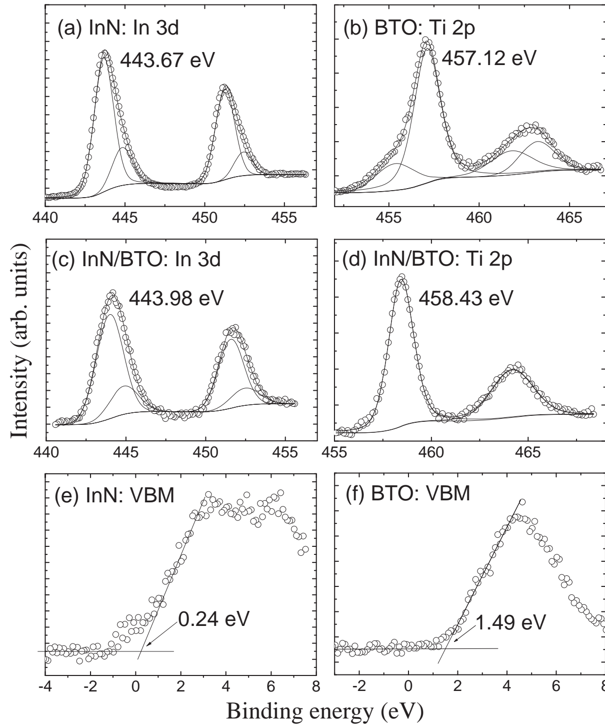


Fig. 12. In 3d spectra recorded on InN (a) and InN/BTO (c), Ti 2p spectra on BTO (b) and InN/BTO (d), and VB spectra for InN (e) and BTO (f). All peaks have been fitted to Voigt line shapes using Shirley background, and the VBM values are determined by linear extrapolation of the leading edge to the base line. The errors in the peak positions and VBM are ±0.03 and ±0.06 eV, respectively.

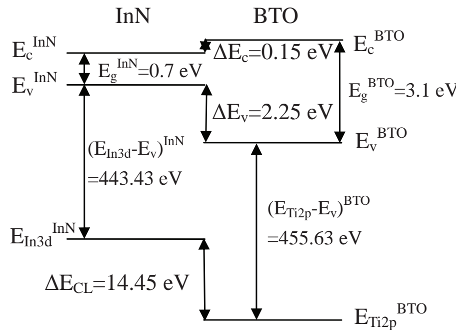


Fig. 13. Energy band diagram of InN/BTO heterojunction.

where $\Delta E_{CL}$=($E_{Ti2p}^{InN/BTO}$-$E_{In3d}^{InN/BTO}$) is the energy difference between In 3d and Ti 2p CLs measured in the thin heterojunction InN/BTO, while ($E_{Ti2p}^{BTO}$-$E_{VBM}^{BTO}$) and ($E_{In3d}^{InN}$-$E_{VBM}^{InN}$) are the VBM energies with reference to the CL positions of bulk BTO and thick InN film, respectively.

Figure 12 shows the XPS Ti 2p and In 3d CL narrow scans and the valence band spectra from the bulk BTO, thick InN and thin InN/BTO samples, respectively. For the In 3d spectra of both the InN and thin InN/BTO samples, additional low intensity higher-binding-energy components were required. These extra components are attributed to In-O bonding due to oxide contamination when InN is present at the surface (Piper et al., 2005), as shown in Fig. 12(a). In the thin InN/BTO sample shown in Fig. 12(c), they are attributed to In-O bonding at the InN/BTO interfaces, and/or inelastic losses to free carriers in the InN layer (King et al., 2008). The CL peak attributed to In-N bonding locates at 443.67±0.03 eV and 443.98±0.03 eV for thick InN and thin InN/BTO, respectively, as shown in Fig. 12(a) and (c). It is interesting that the Ti 2p peaks transform from asymmetry in bulk BTO to symmetry in the thin InN/BTO sample, as observed in the thin ZnO/BTO heterostructure (Jia et al., 2010b). Using the same fitting methods mentioned above, the VBM value for the bulk BTO and thick InN films can be determined, as shown in Fig. 12 (e)and (f). Substituting the above values into Eq. 14, the resulting VBO value is calculated to be 2.25±0.09 eV.

The reliability of the measured result is analyzed by considering several possible factors that could impact the experiment results. Both the CL emissions of In 3d and Ti 2p at the InN/BTO heterojunction are collected from the same surface (InN surface), so the surface band bending effects can be canceled out for the measurement of $\Delta E_{CL}$. Another factor which may affect the precision of the VBO value is the strain-induced piezoelectric field in the overlayer of the heterojunction (Martin et al., 1996). There is a large lattice mismatch of about 7.1% ($\frac{\sqrt{3}a_{InN}-\sqrt{2}a_{BTO}}{\sqrt{2}a_{BTO}}\times 100\%$) between the hexagonal apothem of InN and the BTO[$0\bar{1}1$] direction. It is comparable with that of the InN/ZnO heterojunction (7.7%), and the InN thin film of 5 nm is approximately treated as completely relaxed (Zhang et al., 2007). So the strain-induced piezoelectric field effect can be neglected in our experiment. Thus, the experimental obtained VBO value is reliable.

To further confirm the reliability of the experimental values, it would be useful to compare our VBO value with other results deduced by transitive property. The reported VBO values for ZnO/BTO and InN/ZnO heterojunctions are $\Delta E_V$(ZnO-BTO)=0.48 eV (Jia et al., 2010b), and $\Delta E_V$(InN-ZnO)=1.76 eV (Yang et al., 2009), respectively. Then the $\Delta E_V$(InN-BTO) is deduced to be 2.24 eV, which is well consistent with our measured value 2.25±0.09 eV.

Finally, the CBO ($\Delta E_C$) can be estimated by the formula $\Delta E_C$=$E_g^{BTO}$-$E_g^{InN}$-$\Delta E_V$. By substituting the band gap values at room temperature ($E_g^{InN}$=0.7 eV (Yang et al., 2009) and $E_g^{BTO}$=3.1 eV (Boggess et al., 1990)), $\Delta E_C$ is calculated to be 0.15±0.09 eV. Accordingly, a type-I band alignment forms at the heterojunction interface, as shown in Fig. 13.

## 8. Conclusions

In summary, XPS was used to measure the VBO of the ZnO(or InN)/STO(or BTO) heterojunctions. A type-II band alignment with VBO of 0.62±0.09 eV and CBO of 0.79±0.09 eV is obtained for ZnO/STO heterojunction. A type-II band alignment with VBO of 0.48±0.09 eV and CBO of 0.75±0.09 eV is obtained for ZnO/BTO heterojunction. A type-I band alignment with VBO of 1.13±0.09 eV and CBO of 1.37±0.09 eV is obtained for InN/STO heterojunction. A type-I band alignment with VBO of 2.25±0.09 eV and CBO of 0.15±0.09 eV is obtained for InN/BTO heterojuncion. The accurately determined result is important for the design and application of these semiconductor/ferroelectric heterostructures based devices.

## 9. Acknowledgements

This work was supported by the 973 program (2006CB604908, 2006CB921607), and the National Natural Science Foundation of China (60625402, 60990313).

## 10. References

Alivov Y. I.; Xiao B.; Fan Q.; Morkoc H. & Johnstone D. (2006). *Appl. Phys. Lett.*, Vol. 89, 152115

Amy F.; Wan A. S.; Kahn A.; Walker F. J. & Mckee R. A. (2004). *J. Appl. Phys.*, Vol. 96, 1635

Baer W. S. (1967). *J. Phys. Chem. Solids*, Vol. 28, 677

Boggess T. F.; White J. O. & Valley G. C. (1990). *J. Opt. Soc. Am. B.*, Vol. 7, 2255

Brandt M.; Frenzel H.; Hochmuth H.; Lorentz M.; Grundmann M. & Schubert J. (2009). *J. Vac. Sci. Technol. B*, Vol. 27, 1789

Capasso F. & Margaritondo G. (1987). *Heterojunction band discontinuities: Physics and device applications*, (115-377), Elsevier, 0444870601, North-Holland, Amsterdam Oxford New York Tokyo

Chambers S. A.; Liang Y.; Yu Z.; Droopad R.; Ramdani J & Eisenbeiser (2000). *Appl. Phys. Lett*, Vol. 77, 1662

Chambers S. A.; Liang Y.; Yu Z.; Droopad R. & Ramdani J (2001). *J. Vac. Sci. Technol. A*, Vol. 19, 934

Chen J. J.; Ren F.; Li Y. J.; Norton D. P.; Pearton S. J.; Osinsky A.; Dong J. W.; Chow P. P. & Weaver J. F. (2005). *Appl. Phys. Lett.*, Vol. 87, 192106

Cimalla V.; Lebedev V.; Wang C. Y.; Ali M.; Cke G. E.; Polyakov V. M.; Schwierz F.; Ambacher O.; Lu H. & Schaff W. J. (2007). *Appl. Phys. Lett.*, Vol. 90, 152106

Fan H. B.; Sun, G. S.; Yang S. Y.; Zhang P. F.; Zhang R. Q.; Wei H. Y.; Jiao C. M.; Liu X. L.; ChenY. H.; Zhu Q. S. & Wang Z. G. (2008). *Appl. Phys. Lett.*, Vol. 92, 192107

Foulon Y. & Priester C. (1992). *Phys. Rev. B*, Vol. 45, 6259

Grant R. W.; Waldrop J. R. & Kraut E. A. (1978). *Phys. Rev. Lett.*, Vol. 40, 656

Jia C. H.; Chen Y. H.; Liu G. H.; Liu X. L.; Yang S. Y. & Wang Z. G. (2008). *J. Crystal Growth*, Vol. 311, 200-204

Jia C. H.; Chen Y. H.; Liu G. H.; Liu X. L.; Yang S. Y. & Wang Z. G. (2009). *J. Phys. D: Appl. Phys.*, Vol. 42, 015415

Jia C. H.; Chen Y. H.; Zhou X. L.; Yang A. L; Zheng G. L.; Liu X. L.; Yang S. Y. & Wang Z. G. (2009). *J. Phys. D: Appl. Phys.*, Vol. 42, 095305

Jia C. H.; Chen Y. H.; Zhou X. L.; Liu G. H.; Guo Y.; Liu X. L.; Yang S. Y. & Wang Z. G. (2010). *J. Crystal Growth*, Vol. 312, 373-377

Jia C. H.; Chen Y. H.; Zhou X. L.; Yang A. L.; Zheng G. L.; Liu X. L.; Yang S. Y. & Wang Z. G. (2010). *Appl. Phys. A*, Vol. 99, 511

Jia C. H.; Chen Y. H.; Liu X. L.; Yang S. Y. & Wang Z. G. (2011). *Nano. Res. Lett*, Vol. 6, 316

Kang K. T.; Lim M. H.; Kim H. G.; Kim I. D. & Hong J. M. (2007). *Appl. Phys. Lett.*, Vol. 90, 043502

Kazzi M. E.; Merckling C.; Delhaye G.; Arzel L.; Grenet G.; Bergignat E. & Hollinger G. (2006). *Mater. Sci. Semi. Proc.*, Vol. 9, 954

Kim D.; Choi Y. W. & Tuller H. L., (2005). *Appl. Phys. Lett.*, Vol. 87, 042509

King P. D. C.; Veal T. D.; Jefferson P. H.; Mcconville C. F.; Wang T.; Parbrook P. J.; Lu H. & W.J. Schaff (2007). *Appl. Phys. Lett.*, Vol. 90, 132105

King P. D. C.; Veal T. D.; Lu H.; Hatfield S. A.; Schaff W. J. & Mcconville C.F. (2008). *Surf. Sci.*, Vol. 602, 871

Kryliouk O.; Park H. J.; Won Y. S.; Anderson T.; Davydov A.; Levin I.; Kim J.H. & Freitas Jr. J. A. (2007). *Nanotechnology*, Vol. 18, 135606

Li Y. F.; Yao B.; Lu Y. M.; Li B. H.; Gai Y. Q.; Cong C. X.; Zhang Z. Z.; Zhao D. X.; Zhang J. Y.; Shen D. Z. & Fan X. W. (2008). *Appl. Phys. Lett.*, Vol. 92, 192116

Li Z. W.; Zhang B.; Wang J.; Liu J. M.; Liu X. L.; Yang S. Y.; Zhu Q. S. & Wang Z. G. (2011). *Nano. Res. Lett*, Vol. 6, 193

Lorentz M.; Brandi M.; Schubert J.; Hochmuth H., Wenckstern H. v; Schubert M. & Grundmann M. (2007). *Procc. of SPIE*, Vol. 6474, 64741S

Losurdo M.; Giangregorio M. M.; Bruno G.; Kim T. H.; Wu P.; Choi S.; Brown A.; Masia F.; Capizzi M. & Polimeni A. (2007). *Appl. Phys. Lett.*, Vol. 90, 011910

Losego M. D.; Kourkoutis L. F.; Mita S.; Craft H. S.; Muller D. A.; Collazo R.; Sitar Z. & Maria J. P. (2009). *J. Crystal Growth*, Vol. 311, 1106

Mahboob I.; Veal T. D.; Mcconville C.F.; Lu H. & Schaff W. J. (2004). *Phys. Rev. Lett.*, Vol. 92, 036804

Martin G.; Botchkarev A.; Rockett A. & Morkoc H. (1996). *Appl. Phys. Lett.*, Vol. 68, 2541

Mbenkum B. N.; Ashkenov N.; Schubert M.; Lorentz M.; Hochmuth H.; Michel D.; Grundmann M. & Wagner G. (2005). *Appl. Phys. Lett.*, Vol. 86, 091904

Mönch W. (2004). *Electronic properties of Semiconductor Interfaces*, Springer, Berlin, 176

Mönch W. (2005). *Appl. Phys. Lett.*, Vol. 86, 162101

Murakami H.; Eriguchi K. I.; Torri J. I.; Cho H. C.; Kumagai Y. & Koukitu A. (2008). *J. Crystal Growth*, Vol. 310, 1602

Ozgur U.; Alivov Y. I.; Liu C.; Teke A.; Reshchikov M. A.; Dogan S.; Avrutin V.; Cho S. J. & Morkoc H. (2005). *J. Appl. Phys.*, Vol. 98, 041301

Peruzzi M.; Pedarni J. D.; Bauerle D.; Schwinger W. & Schaffler F. (2004). *Appl. Phys. A.*, Vol. 79, 1873

Piper L. F. J.; Veal T. D.; Walker M.; Mahboob I.; Mcconville C.F., Lu H. & Schaff W. J. (2005). *J. Vac. Sci. Technol. A*, Vol. 23, 617

Siddiqui J.; Cagin E.; D. Chen & Phillips J. D. (2006). *Appl. Phys. Lett.*, Vol. 88, 212903

Singh M.; Wu Y. R. & J. Singh (2003). *Solid State Electron.*, Vol. 47, 2155

Song D. Y.; Holtz M. E.; Chandolu A.; Bernussi A.; Nikishin S. A.; Holtz M. W. & Gherasoiu I. (2008). *Appl. Phys. Lett.*, Vol. 92, 121913

Su S. C.; Lu Y. M.; Zhang Z. Z.; Shan C. X.; Li B. H.; Shen D. Z.; Yao B.; Zhang J. Y.; Zhao D. X. & Fan X. W. (2008). *Appl. Phys. Lett.*, Vol. 93, 082108

Sun H. P.; Tian W.; Pan X. Q.; Haeni J. H. & Schlom D. G. (2004). *Appl. Phys. Lett.*, Vol. 84, 3298

Takahashi N.; Niwa A. & Nakamura T. (2004). *J. Phys. Chem. Solid.*, Vol. 65, 1259

Voora V. M.; Hofmann T.; Schubert M., Brandt M., Lorenz M., Grundmann M., Ashkenov N. & Schubert M. (2009). *Appl. Phys. Lett.*, Vol. 94, 142904

Voora V. M; Hofmann T.; Brandt M.; Lorenz M.; Grundmann M; Ashkenov N.; Schmidt H; Ianno N. & Schubert M. (2010). *Phys. Rev. B*, Vol. 81, No. 19, 195307

Wei X. H.; Li Y. R.; Jie W. J.; Tang J. L.; Zeng H. Z.; Huang W.; Zhang Y. & Zhu J. (2007). *J. Phys. D: Appl. Phys.*, Vol. 40, 7502

Wu C.L.; Shen C. H. & Gwo S. (2006). *Appl. Phys. Lett.*, Vol. 88, 032105

Wu Y. L.; Zhang L. W.; Xie G. L.; Zhu J. L. & Chen Y. H. (2008). *Appl. Phys. Lett.*, Vol. 92, 012115

Yang A. L.; Song H. P.; Liu X. L.; Wei H. Y.; Guo Y.; Zheng G. L.; Jiao C. M.; Yang S. Y.; Zhu Q. S. & Wang Z. G. (2009). *Appl. Phys. Lett.*, Vol. 94, 052101

Yasuda H. & Kanemitsu Y. (2008). *Phys. Rev. B.*, Vol. 77, 193202
You J. B.; Zhang X. W.; Song H. P.; Ying J.; Guo Y.; Yang A. L.; Yin Z. G.; Chen N. F. & Zhu Q. S. (2009). *J. Appl. Phys.*, Vol. 106, 043709
Zhang R. Q.; Zhang P. F.; Kang T. T.; Fan H. B.; Liu X. L.; Yang S. Y.; Wei H. Y.; Zhu Q. S. & Wang Z. G. (2007). *Appl. Phys. Lett.*, Vol. 91, 162104

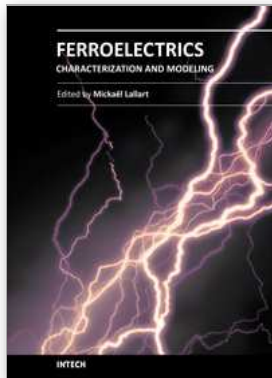


**Ferroelectrics - Characterization and Modeling**
Edited by Dr. MickaÃ«l Lallart

ISBN 978-953-307-455-9
Hard cover, 586 pages
**Publisher** InTech
**Published online** 23, August, 2011
**Published in print edition** August, 2011

Ferroelectric materials have been and still are widely used in many applications, that have moved from sonar towards breakthrough technologies such as memories or optical devices. This book is a part of a four volume collection (covering material aspects, physical effects, characterization and modeling, and applications) and focuses on the characterization of ferroelectric materials, including structural, electrical and multiphysic aspects, as well as innovative techniques for modeling and predicting the performance of these devices using phenomenological approaches and nonlinear methods. Hence, the aim of this book is to provide an up-to-date review of recent scientific findings and recent advances in the field of ferroelectric system characterization and modeling, allowing a deep understanding of ferroelectricity.

**How to reference**
In order to correctly reference this scholarly work, feel free to copy and paste the following:

Caihong Jia, Yonghai Chen, Xianglin Liu, Shaoyan Yang and Zhanguo Wang (2011). Valence Band Offsets of ZnO/SrTiO3, ZnO/BaTiO3, InN/SrTiO3, and InN/BaTiO3 Heterojunctions Measured by X-Ray Photoelectron Spectroscopy, Ferroelectrics - Characterization and Modeling, Dr. MickaÃ«l Lallart (Ed.), ISBN: 978-953-307-455-9, InTech, Available from: http://www.intechopen.com/books/ferroelectrics-characterization-and-modeling/valence-band-offsets-of-zno-srtio3-zno-batio3-inn-srtio3-and-inn-batio3-heterojunctions-measured-by-

INTECH
open science | open minds

**InTech Europe**
University Campus STeP Ri
Slavka Krautzeka 83/A
51000 Rijeka, Croatia
Phone: +385 (51) 770 447
Fax: +385 (51) 686 166
www.intechopen.com

**InTech China**
Unit 405, Office Block, Hotel Equatorial Shanghai
No.65, Yan An Road (West), Shanghai, 200040, China
中国上海市延安西路65号上海国际贵都大饭店办公楼405单元
Phone: +86-21-62489820
Fax: +86-21-62489821

© 2011 The Author(s). Licensee IntechOpen. This chapter is distributed under the terms of the Creative Commons Attribution-NonCommercial-ShareAlike-3.0 License, which permits use, distribution and reproduction for non-commercial purposes, provided the original is properly cited and derivative works building on this content are distributed under the same license.